AAPS PharmSciTech (2023) 24:123
https://doi.org/10.1208/s12249-023-02583-y

RESEARCH ARTICLE

In Vitro Prototyping of a Nano-Organogel for Thermo-Sonic Intra-Cervical Delivery of 5-Fluorouracil-Loaded Solid Lipid Nanoparticles for Cervical Cancer

Samson A. Adeyemi[1] · Zardad Az-Zamakhshariy[1] · Yahya E. Choonara[1]

Received: 6 March 2023 / Accepted: 8 May 2023 / Published online: 24 May 2023

Abstract
Solid lipid nanoparticles (SLNs) are used extensively to achieve site-specific drug delivery with improved bioavailability and reduced toxicity. This work focused on a new approach to provide site-specific stimuli-responsive delivery of SLNs loaded within thermo-sonic nano-organogel (TNO) variants to deliver the model chemotherapeutic agent 5-FU in treating cervical cancer. Pharmaceutically stable nanospherical SLNs comprising poly-L-lactic acid (PLA), palmitic acid (PA), and polyvinyl alcohol (PVA) were prepared and incorporated into TNO variants augmented by external thermal and ultrasound stimuli for release of 5-FU in the cervix. Results revealed that rate-modulated 5-FU release was achieved from SLNs (particle size =450.9 nm; PDI =0.541; zeta potential =−23.2 mV; %DL =33%) within an organogel upon exposure to either a single (thermo-) and/or both (thermo-sonic) stimuli. 5FU was released from all TNO variants with an initial burst on day 1 followed by sustained release over 14 days. TNO 1 provided desirable release over 15 days (44.29% vs. 67.13% under single (T) or combined (TU) stimuli, respectively). Release rates were primarily influenced by the SLN:TO ratio in tandem with biodegradation and hydrodynamic influx. Biodegradation by day 7 revealed that variant TNO 1 (1:5) released 5FU (46.8%) analogous to its initial mass than the other TNO variants (i.e., ratios of 2:5 and 3:5). FT-IR spectra revealed assimilation of the system components and corroborative with the DSC and XRD analysis (i.e., in ratios of PA:PLA 1:1 and 2:1). In conclusion, the TNO variants produced may be used as a potential stimuli-responsive platform for the site-specific delivery of chemotherapeutic agents such as 5-FU to treat cervical cancer.

Keywords cervical cancer · organogels · solid lipid nanoparticles · sustained release · thermal and ultrasound stimuli · 5-fluorouracil

Introduction

The establishment of nanomedicine has revolutionized advances in chemotherapy for oncology [1, 2]. Nano-enabled drug delivery systems continue to progress as an efficient therapeutic approach using various nanostructures such as nanoparticles, nanomicelles, or nanoliposomes [3–6]. For example, the chemotherapeutic agent 5-flourouracil (5FU) has been successfully used as adjunct drug therapy to treat cervical cancer, and recent research has shown that when applied locally within nanolipids, it provides enhanced drug loading and controlled-release chemotherapy for women diagnosed with cervical intraepithelial neoplasia 2 (CIN II) [7, 8].

Similarly, solid lipid nanoparticles (SLNs) are widely used to achieve site-specific drug delivery with superior bioavailability [9]. SLNs provide an augmented drug encapsulating capacity during formulation and surface functionalization can occur for the targeted delivery of bioactives [10]. SLNs also have a superior structural stability profile owing to the arrangement of the lipophilic core and the singular phospholipid layer bordering the nanostructure [11]. In most instances, drug release from SLNs is biphasic which includes an initial burst and thereafter a controlled drug release phase [12].

However, a disadvantage of SLNs used in chemotherapeutic applications is their rapid clearance from the body.

✉ Yahya E. Choonara
yahya.choonara@wits.ac.za

[1] Wits Advanced Drug Delivery Platform Research Unit, Department of Pharmacy and Pharmacology, School of Therapeutic Science, Faculty of Health Sciences, University of the Witwatersrand, Johannesburg, South Africa

Hence, incorporating SLNs within responsive carrier gels to prolong the release or circulation of drug-loaded SLNs has also been demonstrated as a viable approach [13]. The polymeric structure of the carrier gel determines the release profile of the drug-loaded SLNs from the gel. It is worth noting that the physicomechanical properties of the gel, for example, elasticity, can provide rate-modulating release in comparison to native SLNs [14].

Conventional gels used to carry SLNs have a fibrous network comprising gelators that support the solvent molecules and therefore display sponge-like viscoelastic properties [15]. Alternatively, organogels are a class of gels constituting a liquid organic phase embedded within a three-dimensional crosslinked network. Organogels can be synthesized via conventional gel network formations through polymerization. A self-assembly strategy can also be employed to form low molecular weight organogel networks that are thermodynamically stable for drug delivery applications [16]. A number of secondary forces, including hydrogen bonding and van der Waals forces, facilitate the clustering of monomers into non-covalently bonded networks that restrain organic solvent and display gel-like physical properties with network growth [16].

Furthermore, advancing organogels for biomedical applications has gained much interest. For instance, through the use of ultrasound-responsivity, a unique approach for site-specific drug delivery can be achieved to overcome the impeding challenges that physiological barriers (e.g., at the cervix) pose to the efficient delivery of high molecular weight chemotherapeutic agents and/or molecules that are poorly soluble [17].

Native ultrasonic energy has been used to treat specific medical conditions, including tumoral ablation. In addition, ultrasound-mediated therapy has been shown to increase the safety and efficacy of chemotherapeutic agents through cavitation and drug diffusion into tumoral tissue [18, 19]. Its use can facilitate and/or augment drug release leading to higher drug accumulation within the diseased tissue/s by promoting focused therapy. A combination of thermal and mechanical (thermo-mechanical) properties through the use of ultrasound can also enhance the delivery of chemotherapeutic drugs without microbubbles by the vaporization of gas-precursors [20].

The gold standard treatment for cervical cancer includes complicated surgical intervention, non-targeted intravenous chemotherapy, and/or cytotoxic radiotherapy either alone or in combination. The use of palliative chemotherapy improves quality of life by relieving disease symptoms, but it is not efficient in decreasing tumor size [21].

Hence, there is a need for a more site-specific treatment option for the efficient treatment of cervical cancer by having a delivery system providing sustained intracervical drug release. In keeping with the approaches described earlier, this work focused on the facile synthesis of 5FU-loaded SLNs prepared via a spray-drying technique followed by incorporating them into a thermosonic organogel matrix as a direct intracervical injectable chemotherapy. Detailed physicochemical analysis of native SLNs and the SLN-loaded thermosonic organogel system was undertaken including assessment of the 5FU release profiles at different ratios of SLNs within the formulation as a potentially viable option for the site-specific delivery of 5-FU in treating cervical cancer.

Materials and Methods

Materials

Poly-L-lactic acid (PLA), palmitic acid (PA), poly(vinyl alcohol) (PVA), dichloromethane (DCM), methanol, 5-Fluorouracil (5-FU), ethylene glycol (EG), ethanol, dimethyl sulfoxide (DMSO), N-(Isopropyl Acrylamide) (NIPAM), sebacic acid (SA), 1,3 4-(carboxyphenoxy) propane (CPP), sodium dodecyl sulfate (SDS), methylene bis-acrylamide (MBA), and ammonium persulfate (APS) were purchased from Sigma-Aldrich Inc. (St. Louis, MO, USA).

Preparation of Thermosonic Organogel (TO) Variants

TO1: N-Isopropyl Acrylamide and Sebacic Acid

NIPAM (300 mg) was dissolved in 5 mL of ethylene glycol, and a sebacic acid (25 mg) solution (125 mL DMSO) was separately prepared before adding it drop-wise to the NIPAM solution to form an emulsion stabilized by sodium dodecyl sulfate (7 mg). Methylene bis-acrylamide (135 mg) was then added to the solution (12:1:5:7/50) and allowed to dissolve under sealed inert conditions and stirred with the addition of ammonium persulfate (10% w/v) to complete the reaction before the gelling time was recorded. TO1 was then refrigerated at 5°C to stabilize.

TO2: N-Isopropyl Acrylamide and 1,3 4-(Carboxyphenoxy) Propane

NIPAM (300 mg) was dissolved in 5 mL of ethylene glycol while 1,3 4-(carboxyphenoxy) propane (CPP) (25 mg) was separately dissolved in 0.25 mL of DMSO under mild heating (30°C). The CPP solution was added to the NIPAM solution in a drop-wise manner to form a turbid (white) emulsion stabilized by sodium dodecyl sulfate (7 mg). Methylene bis-acrylamide (90 mg) was added to the solution (12:1:1:3/10:7/50) under inert conditions until TO2 formation was achieved, and the reaction gelling time was recorded. TO2 was then refrigerated at 5°C to stabilize.

TO3: N-Isopropyl Acrylamide, Sebacic Acid, and 1,3 4-(Carboxyphenoxy) Propane

NIPAM (300 mg) was dissolved in 5 mL of ethylene glycol while sebacic acid (25 mg) and 1,3 4-(carboxyphenoxy) propane (CPP) (25 mg) solutions were prepared separately under mild heating (30°C). The CPP solution was added drop-wise to the sebacic solution forming a turbid emulsion that was added drop-wise to the NIPAM solution. The system was stabilized with sodium dodecyl sulfate (7 mg). Methylene bis-acrylamide (90 mg) was then added to the emulsion (12:1:3/10:7/50) to achieve TO3 formation and the reaction gelling time was recorded. TO3 was then refrigerated at 5°C to stabilize.

Synthesis of the 5FU-Loaded Solid Lipid Nanoparticles (SLNs)

Two variants of SLNs were prepared, i.e., a 1:1 and 2:1 ratio of poly-l-lactic acid (PLA): palmitic acid (PA) (PA:PLA). Equal weights of PA (25 mg) and PLA (25 mg) were simultaneously dissolved in 10 mL of DCM. 5-FU (25 mg) was dissolved in methanol (2 mL) and added to the PA:PLA polymeric solution under agitation. Simultaneously, a 1% solution of PVA as a stabilizer was added under rapid stirring (400 rpm) using a thin stream technique [22] and allowed to stir until minimal precipitation occurred to coat the SLNs. The resultant mixture was then filtered (0.8 µm pore size) and collected in a conical flask before passing through a Nano Spray Dryer (Buchi Nano Spray Dryer B-90, Switzerland) using a 5-µm nozzle set at a gas flow rate = 112 L/min, inlet temperature = 50°C, outlet temperature = 36°C, head temperature = 63°C, degree of spray = 85%, pressure = 34 mBar and a pump level set at a value of 2. These settings were applied to the synthesis of both SLN variants (i.e., 1:1 and 2:1 PA:PLA, respectively). Solutions fed through the Nano Spray Dryer resulted in an off-white free-flowing powder obtained at the collecting chamber that was prepared for further characterization and optimization of the PA:PLA ratio, particle size, morphology, 5FU loading efficiency, and assimilation within the preferred Thermosonic Organogel variant.

Assembly of SLNs and TO Variants to Form a Thermosonic Nano-Organogel (TNO)

The prepared 5FU-loaded SLNs were physically blended with a subsequent open ring reaction into the Thermosonic Organogel/s based on varying ratios. Three TO formulations (TO1, TO2, and TO3) were prepared corresponding to three concentrations of SLNs in ratios of 1:5, 2:5, and 3:5 totaling nine samples of the combined nanosystem. The SLNs were dispersed within the TO formulations via mechanical stirring of the mixture until dispersion occurred before initiating the open ring reaction of the gel. The mixture was then reacted in a sealed vessel under N_2 atmosphere kept at 50°C to form a thermosonic nano-organogel (TNO).

Probing the Molecular Integrity of the TNO Formulation

Fourier transform infrared (FT-IR) spectroscopy was undertaken on the native polymers and the newly synthesized TNO variants to investigate the chemical structure stability and detect newly arranged bonds or structural integrity changes as a result of TNO formation from the native polymers. A Perkin Elmar Spectrum 2000 FT-IR (Llantrisant, Wales, UK) fitted with a universal ATR polarization accessory at a 4-cm^{-1} resolution was used and a conical probe was attached for reading all samples (N=3) set at 10 scans with a force gauge set at a 120 psi. All readings were scanned and analyzed in the range of 4000 to 600 cm^{-1}.

Analysis of the Thermal Stability of the TNO Formulation

The thermal activity of the SLNs was analyzed using a Mettler-Toledo, DSC1 STAR^e (Schwerzenback, Switzerland) differential scanning calorimeter (DSC). The native (PA, PLA) (10 mg) and blended polymers (PA-PLA) (5 mg) were weighed into aluminum crucible pans that were sealed within pinhole crucibles. The crucibles were positioned and calibrated individually according to weight and exposed to a temperature ramp of 10°C/min between 20 and 500°C under a constant N_2 atmosphere. Outcomes of the thermal events by each sample were presented by thermograms that were analyzed.

Determination of the Molecular Phase Transitions of the TNO Formulation

The molecular (re) arrangement of the native polymers and the composite nanosystem was determined using a benchtop X-Ray Diffractometer (MiniFlex600 XRD, Rigaku Corp., Tokyo, Japan) incorporated with a high-intensity D/tex ultra-high speed 1D detector, a 600 W X-ray generator, and a counter monochromator. The XRD profiles of each sample (i.e., PA, PLA, and PA-PLA blends) were analyzed with phase determination of each sample correlated by the peak intensity presented in the DSC thermograms.

Investigation of the Morphology of the TNO Formulation

The structural morphology of the TNO variants were analyzed and confirmed using a Carl Zeiss Sigma Field

Emission SEM equipped with an Oxford x-act EDS detector (Carl Zeiss SEM, England). Samples were prepared by attaching a double-sided carbon tape to stub holders and lightly applying samples of the SLNs across the surface area before coating with palladium-gold and loaded into the SEM to be viewed and analyzed.

Determination of the 5FU Loading Efficiency within the SLN's

Serial dilutions of 5FU in PBS (pH 7.4; 37°C) were prepared in triplicate (N=3) and transferred individually to quarts cuvettes before scanning using a UV spectrophotometer set at the λ_{max} for 5FU (230 nm). A calibration curve (r^2=0.9) was used to interpret the results obtained. The 5FU-loaded SLNs in ratios of 1:1 and 2:1 were then completely dissolved in methanol and analyzed for the 5FU entrapment efficiency (% DEE) calculated using Eq. 1 where the % drug loading for each formulation was calculated [23]. Equation 2 was used to calculate the drug encapsulation efficiency (%DEE) [24]:

$$\%DL = \frac{Weight\ of\ drug\ in\ formulation}{Total\ weight\ of\ formulation} \times 100 \quad (1)$$

$$\%DEE = \frac{Actual\ amount\ of\ drug\ loaded}{Theoretical\ amount\ of\ drug\ loaded} \times 100 \quad (2)$$

Determination of the Micromeritic Properties of the SLNs

The particle size, surface charge (zeta potential), and polydispersity index (PDI) of the SLNs were analyzed using dynamic light scattering (ZetaSizer NanoZS, Malvern Instruments, UK). Samples (2 mg) of SLNs were diluted in 5 mL of distilled water and ultrasonicated for 30 s to form a stable dispersion. Each sample was then transferred into disposable cuvettes and simultaneously analyzed for particle size and the PDI value. A mean of 30 scans were captured before the profiles were produced, and samples from the stock dilutions were also used to assess the zeta potential using a folded capillary cell.

Evaluation of the Biodegradation and Hydrodynamics of the TNO Formulation

Biodegradation trials were undertaken with 12 samples of the TNO formulation with the initial weights recorded. The samples were then suspended in acetate buffer pH 4.3 in 100 mL vessels and placed in an orbital shaking incubator (50 rpm; 37°C). Sample weights were recorded on days 1, 3, and 7. At each time point, any additional residue was removed prior to weighing, and profiles were constructed to decode the biodegradation and hydrodynamic (swelling/shrinking) behavior of the TNO formulations.

Determination of 5FU Release from the Native SLNs and the TNO Formulation

A total of 20 TNO samples (i.e., two groups of 10 formulations each) were prepared for the 5FU release studies. Group 1 was tested for thermo-responsivity while Group 2 was tested for simultaneous thermo- and ultrasound-responsivity. Each group comprised 9 TNO formulation samples and 1 control group of native SLNs. The samples were sealed in dialysis tubing and suspended in simulated cervical fluid (SCF) (100 mL acetate phosphate buffer) before being placed in an orbital shaking incubator (25 rpm; 37°C). At each time interval, 5 mL of the SCF was withdrawn from each sample vessel for analysis. Samples in Group 2 were exposed to ultrasound (1 MHz; 10 s) before sample withdrawal [25, 26]. 5FU-free SCF release media was replaced at each sample withdrawal to maintain sink conditions. All samples were scanned by UV absorption (230 nm), and the results were used to compute the 5FU release profiles for each group to determine the pattern of drug release in the presence of the thermos and ultrasound stimuli.

Results and Discussion

Assessment of the Surface Morphology and Micromiretic Properties of the SLN's

The surface morphology, particle size, and shape of the SLNs conformed to stable nanoconstructs having patent features. Figure 1 depicts two formulation variants, i.e., 1:1 PA:PLA and a 2:1 PA:PLA with and without 5FU loading. By analyzing the particle shape and surface area, it was confirmed that concentrically smooth spherical particles were produced with a significant yield at the nanoscale (nanospheres). SEM imagery was used to demarcate (Da x) and measure (nm) the particle dimensions. In Fig. 1a, annotations on two particles (Da1=279.2 nm and Da2=509.1 nm) reveal a heterogeneous particle population stabilized by the increase in surfactant [27]. In comparison to Fig. 1a (i.e., 5FU-loaded SLNs), Fig. 1b showed significantly smaller particles averaging only 181.6 nm. Abbaspour and co-workers (2013) [28] reported that the particle size proportionately increases when ionic complexed chemotherapeutic drugs are encapsulated within SLNs and based on the polymer concentration. When analyzing Fig. 1c (higher polymer concentration at 2:1), significantly larger particle sizes (Da1=666.3 nm and Da2=450.7 nm) were obtained compared with Fig. 1a. The average particle size of the SLNs annotated

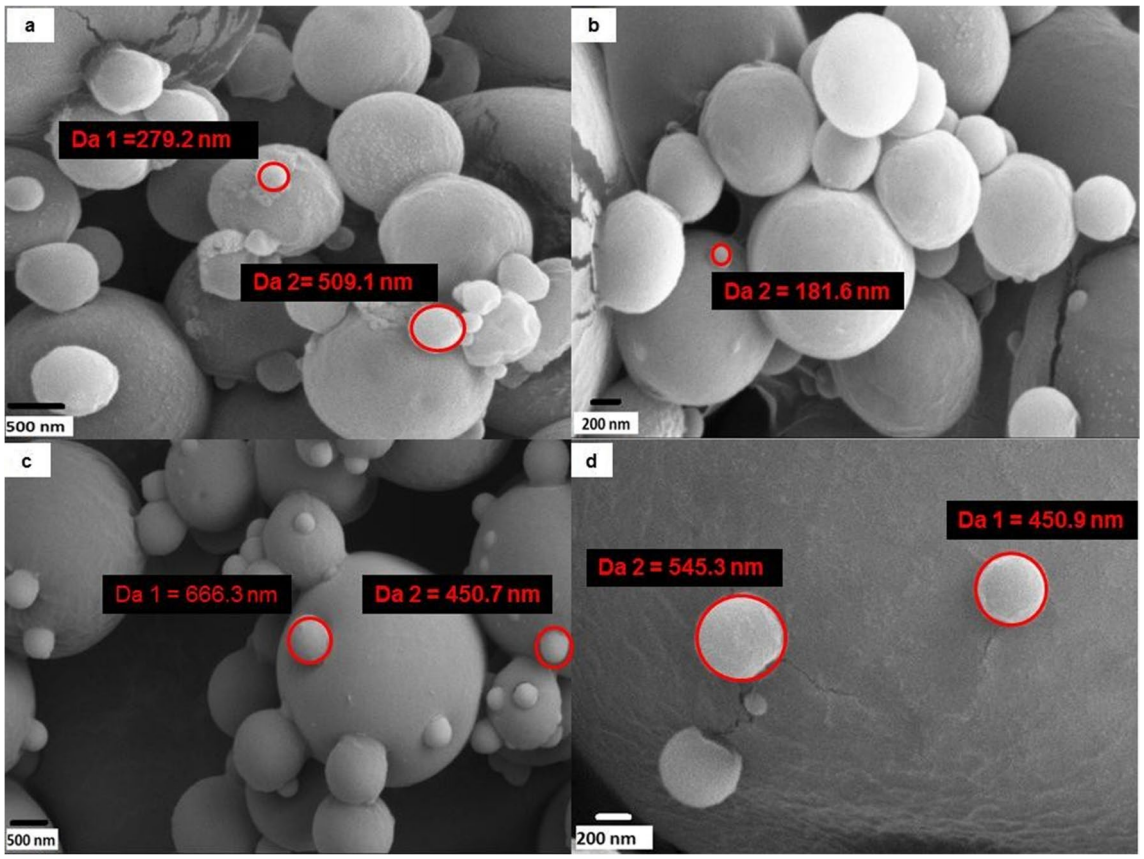

Fig. 1 Annotated scanning electron microscopy images for **a** 1:1 PA:PLA (drug encapsulated) (typical lowest particle size indicated at 279.2 nm), **b** 1:1 PA:PLA (drug-free) (typical lowest particle size indicated at 181.6 nm), **c** 2:1 PA:PLA (drug encapsulated) (typical lowest particle size indicated at 450.7), and **d** 2:1 PA:PLA (drug-free) (typical lowest particle sizes indicated at 450.9 nm)

and visible in Fig. 1d was recorded at Da1=450.9 nm and Da2=545.3 nm.

The surface charge (zeta potential) and particle sizing of the SLNs were also assessed by dynamic light scattering for the different formulation variants. The target PDI value was set at <0.7 to ensure stability and an acceptable particle size distribution [29, 30]. Figure 2a illustrates the relative yield of SLNs that fall within the desired particle size range. A

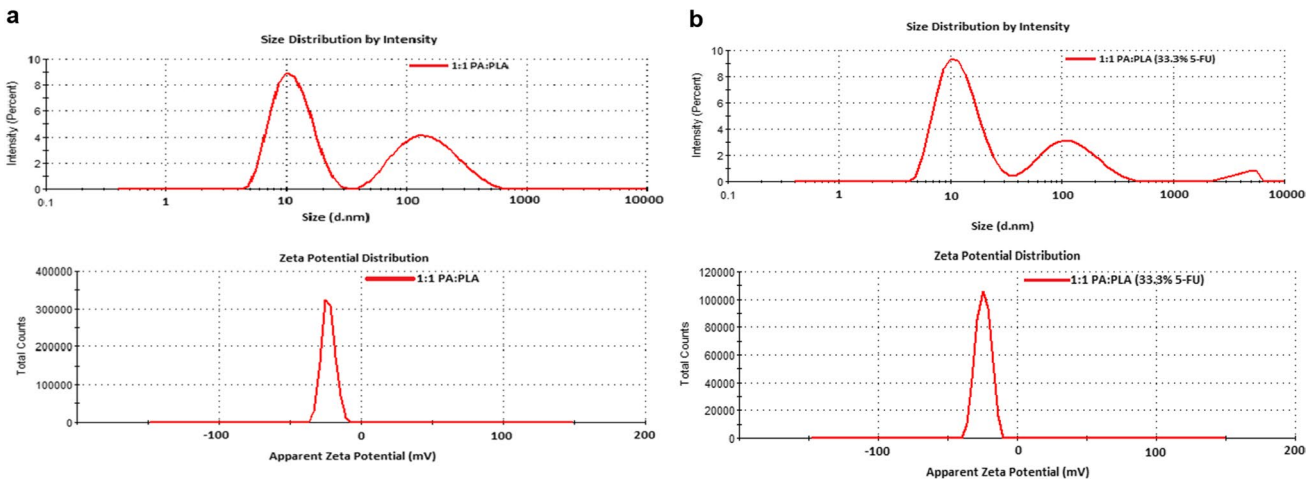

Fig. 2 Graphs depicting zeta size and zeta potential for **a** 1:1 PA:PLA (plain) and **b** 1:1 PA:PLA (drug encapsulated)

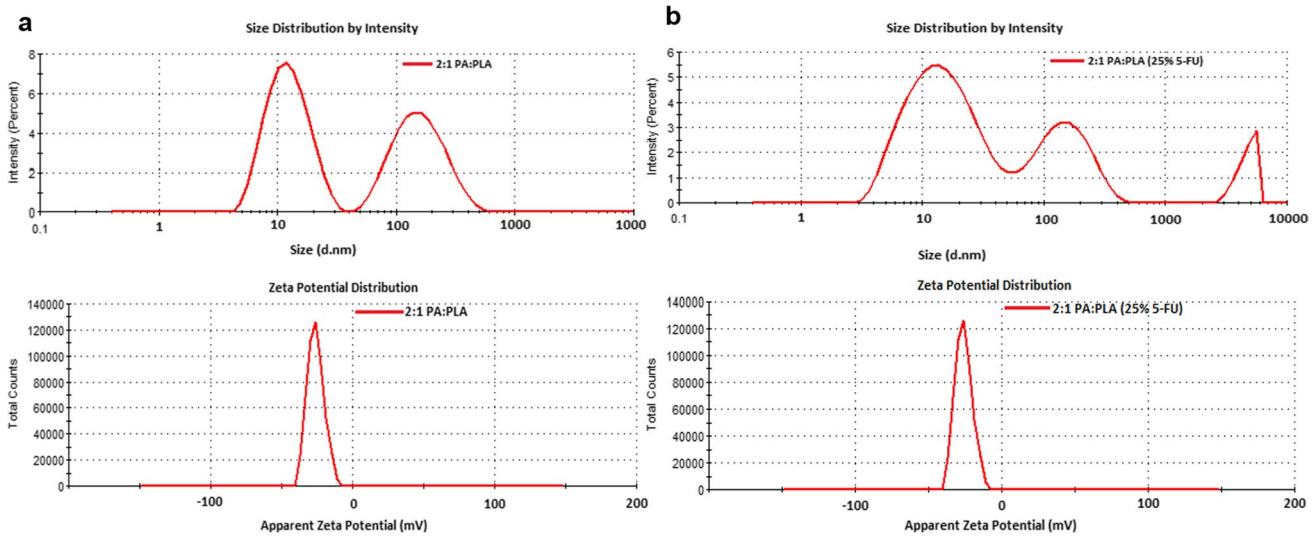

Fig. 3 Graphs depicting zeta size and zeta potential for **a** 2:1 PA:PLA (plain) and **b** for 2:1 PA:PLA (drug encapsulated)

large proportion of particles were recorded at 11.72 d.nm (size) with a 58.1% intensity with 41.9% of particles in the range of 167.4 d.nm, revealing a typical bi-modal particle size distribution. The 1:1 PA:PLA variant recorded a PDI value of 0.541 and a stable zeta potential at −23.2 mV.

The 5FU-loaded SLNs typically revealed a larger size range than the pure SLNs with tri-modal distribution Fig. 2b. Majority of particles (60.9%) were recorded at 11.99 d.nm, followed by 36% at 155 d.nm and 3.1% at 523.3 d.nm. The PDI of the 1:1 PA:PLA variant was recorded at 0.151 indicating a desirable size distribution with a zeta potential value of −24.6 mV indicating particle stability.

As reported by Honary and Zahir (2013) [31], cationic chitosan-modified-paclitaxel-PLGA nanoparticles promoted an electrostatic interaction with cancerous cells due to an anionic surface of tumor tissue; hence, a greater accumulation of the nanoparticles occurred at the tumor site for passive intracellular uptake. However, Grainger and co-workers (2010) [32] reported that anionic nanoparticles may also be ideal for cancerous tissue as they move rapidly through the interstitium due to repulsive forces and settle between the matrix of the cell walls. In addition, pulsatile ultrasound to be applied to the SLNs synthesized in this study may further enhance the nanoparticle penetration at cancerous tissue in the cervix.

Figure 3a reveals a bi-modal particle size distribution for the 2:1 PA:PLA SLNs. Majority of particles (55%) were recorded at 12.92 d.nm with 45% at 169.9 d.nm. On average, the particle size was computed at 19.60 d.nm with a PDI value of 0.597. This suggested that the higher the polymer concentration (2:1), the larger particle sizes were obtained. The zeta potential values >30 mV are also known to retain desirable stability, and values approaching ±60 mV are considered outstanding stability [33]. It was noted that the zeta potential value for the 2:1 PA:PLA (5-FU free) variant was −26.2 mV with reasonable stability. Figure 3b shows that as with the 1:1 PA:PLA 5-FU-loaded variant, the 2:1 PA:PLA 5-FU-loaded formulation revealed three peaks ranging higher than the 1:1 PA:PLA variant. This was due to the higher concentration of the polymer component (i.e., 2:1) in these SLNs. Majority of the particles (62.6%) were recorded at 16 d.nm with 29.4% at 472 d.nm and a PDI value of 0.307. These results suggest ideal colloidal stability from a particle size and zeta potential (−25.2 mV) perspective. Further stability improvements can be made by the addition of alternative surfactants (type and quantity) if required [34, 35].

Chemical Structure Stability Analysis of the SLNs

FT-IR spectroscopy of the native polymers as well as the 5FU-loaded and pure SLNs was completed to assess the chemical structure and molecular stability of the SLNs synthesized. Figure 4a reveals the C-H stretch bands between 2937 and 2940 cm^{-1} of palmitic acid (PA) and a prominent band at 1695 cm^{-1} confirming the presence of the COOH functional group of PA. Poly-l-lactic acid (PLA) comprises various prominent peaks, one of which appears at 1752 cm^{-1} representing the C=O of the strong ester backbone of PLA. Other peaks include the 1085 cm^{-1} and 1182 cm^{-1} also suggesting C-O ester groups. Poly(vinyl alcohol) (PVA) was used to coat the SLNs during formulation. By analyzing the IR spectra for PVA in Fig. 4b, a broad band was noted between 3027 and 3614 cm^{-1} attributed to hydrogen-bonded alcohols (OH). In addition, a C-H stretch band at 2942 cm^{-1} and further down the spectrum revealed a strong carbonyl band at 1729 cm^{-1}. A low-intensity peak at 1376 cm^{-1} and a larger band at 840 cm^{-1} are reported to be C-H wagging

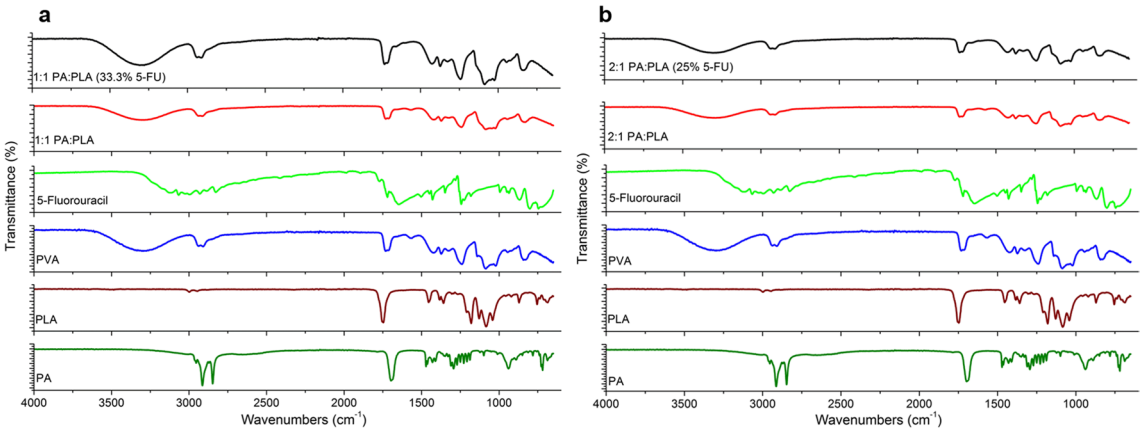

Fig. 4 Graph illustrating the surface molecular status of **a** 1:1 PA:PLA plain and 1:1 PA:PLA drug encapsulated and **b** 2:1 PA:PLA (plain) and 2:1 PA:PLA (drug encapsulated)

and C-H rocking bands, respectively [36]. The broad band between 2750 and 3250 cm^{-1} spectrums confirmed the presence of an amine as stretching bands around 3000–3500 cm^{-1}. These spectrums were attributed to the -NH stretching vibrations in the spectrum of 5-FU signifying its incorporation into the formulation. A band at 1250 cm^{-1} indicated a CF stretch band representing the carbon-fluoride bond in 5-FU [37]. Lastly, analysis of the FT-IR spectra shown in Fig. 4 revealed assimilation to the spectrum of PVA except for peak intensity, substantiating the PVA coating. Results from both formulation variants (i.e., ratios of PA:PLA 1:1 and 2:1) revealed corroborative data.

Thermal Stability Behavior of the Various Components of the SLNs

DSC analysis on the native polymers and the formulated SLNs revealed the thermal stability of the various blended components and the SLNs. Figure 5a shows a melting point for PA at 68.59°C conforming to the data reported by Latibari and co-workers (2014) [38]. A visible exothermic peak was noted representing oxidative degradation. When observing the thermogram of PLA, a first thermal event occurred at 184.89°C and with another at 190.25°C signifying the Tg of PLA. At 358.86°C, a broad exothermic peak representing the amorphous PLA Mpt. PVA has a Tg at 57.04°C with crystallization at 276.32°C before a broad exothermic peak signifying its Mpt at 323.39°C. When analyzing 5-FU, a sharp thermal peak at 278.09°C revealed the Mpt, and at 349.14°C, cold crystallization proceeded. A similar thermal pattern between pure PVA and the SLNs was noted due to the high PVA concentrations used as a coating Fig. 5b. The thermograms representing the SLNs generally showed a lower Mpt than pure PVA. Specifically for the SLNs, it was noted that the 5FU-loading showed a lower Mpt and less peak intensity than the pure SLNs with thermal activity at 472.45°C and 479.64°C for the 1:1 PA:PLA (25% 5-FU) and 2:1 PA:PLA (33.3% 5-FU), respectively.

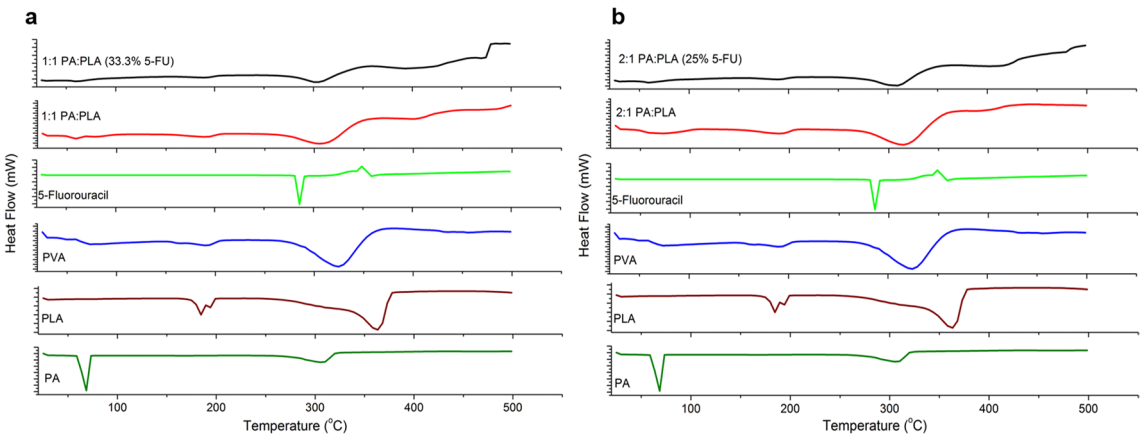

Fig. 5 Graph illustrating the thermal behavior for **a** 1:1 PA:PLA (plain) and 1:1 PA:PLA (drug encapsulated) and **b** 2:1 PA:PLA (plain) and 2:1 PA:PLA (drug encapsulated)

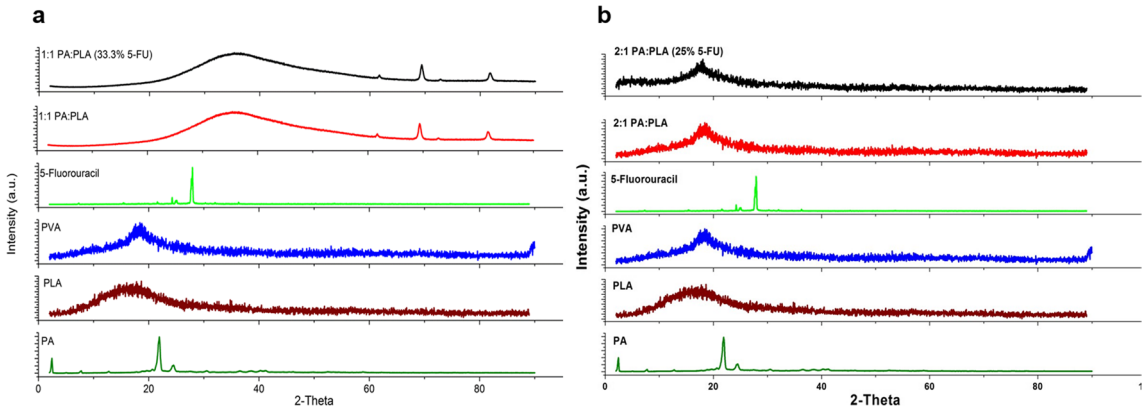

Fig. 6 Molecular phase classification of **a** 1:1 PA:PLA (plain) and 1:1 PA:PLA (drug encapsulated) and **b** 2:1 PA:PLA (plain) and 2:1 PA:PLA (drug encapsulated)

Ordering the Molecular Phase Transitions of the SLNs

Molecular phasing was ordered by XRD profiles generated and for each polymer and their combinations. Results were integrated with the DSC data obtained to draw deeper inference. Analyzing the XRD profiles from Fig. 6a and b, PA had three peaks with the first occurring at 2.42° at an intensity of 3809.80 a.u. The second peak presented a sharp intense peak of 9824.67 a.u. at 21.74° and the third at 24.62° with an intensity of 1997.55 a.u. This data conforms to earlier results reported by Latibari and co-workers on PA (2014) [38]. The sharp intensity peaks revealed that PA had a crystalline lattice structure corroborating with the DSC data on the intense melting point peak. A broad peak was recorded for PLA at 16.99° with low intensity (56.06 a.u) signifying an amorphous molecular structure as corroborated by the broad DSC peak. The XRD profile of PVA showed a broad peak at 19° with low intensity (45.63 a.u) indicating the amorphous molecular arrangement of PVA [39]. Evaluating the XRD profile of 5-FU revealed a sharp intense peak of 1086.79 a.u. at 28° indicating the typical crystallinity of the drug [40].

Interestingly, when analyzing the XRD profiles of the pure SLNs, there was a broad intense peak of 5562.86 a.u. at 35.63° and an intensity peak of 5493.78 a.u. at 35.29° with sharp peaks at 69.36° and 81.73°. This indicated that the SLNs had a semi-crystalline structure Fig. 6a. In Fig. 3b, the XRD profiles of 5-FU-loaded SLNs had a broad band of low intensity (61.35 a.u) at 17.67° while 58.89 a.u at 18.35° for the pure SLNs. This confirmed the amorphous nature for the SLNs at a 2:1 PA:PLA ratio.

Assessment of the 5-FU Loading and Encapsulated Efficiency Within the SLNs

The 5-FU loading (%DL) within the two variants of SLNs was computed as 33% and 25% for the PA:PLA 1:1 and 2:1 ratios, respectively. The %DEE of the 1:1 and 2:1 PA:PLA variants were calculated as 58.29% and 34.11%, respectively. Results are reported as a mean of triplicates (N=3) for all measurements.

Evaluation of the Biodegradation and Hydrodynamic Profiling of the TNO System

There exists a very strong relationship between the pore structure and the chemical interactions of the variants and the nanogels as exemplified [41, 42]. The varied starting points of the different formulations influenced their biodegradation and subsequently facilitates 5FU release patterns within their unique matrixes Fig. 7.

Biodegradation studies proceeded by exposing the formulation variants to bio-relevant media (i.e., simulated cervical fluid (SCF)). On day 1 of the biodegradation study, a significant increase in weight was observed for all formulation variants indicating gelation (swelling) followed by a gradual stabilization of biodegradation, for example, reaching a maximum weight of 2565.69 mg after 7 days for the TNO 1 (2:5) variant. Comparative analysis of formulations TO1 and TNO1 revealed a similar trend of initial weight increase attributed to fluid absorption between days 1 and 3 followed by stabilized biodegradation. Interestingly, for variants 3:5 of TNO 2 and TNO 3 (between days 3 and 7), a relative increase in weight was recorded. Biodegradation by day 7 revealed that the weight of the TO and TNO formulations deviated from the initial mass recorded and corroborated with the 5FU release profiles in SCF. On day 7, variant TNO 1 (1:5) released the highest concentration of 5FU (46.8%) analogous to its initial weight and at a higher rate than the other TNO variants whereas variants of TNO 1 (i.e., 2:5 and 3:5) showed a slower 5FU release pattern, i.e., 23.8% and 21.8%, respectively. This corresponds to a slower biodegradation rate over variant TNO 1 (1:5). Figure 7b indicates that

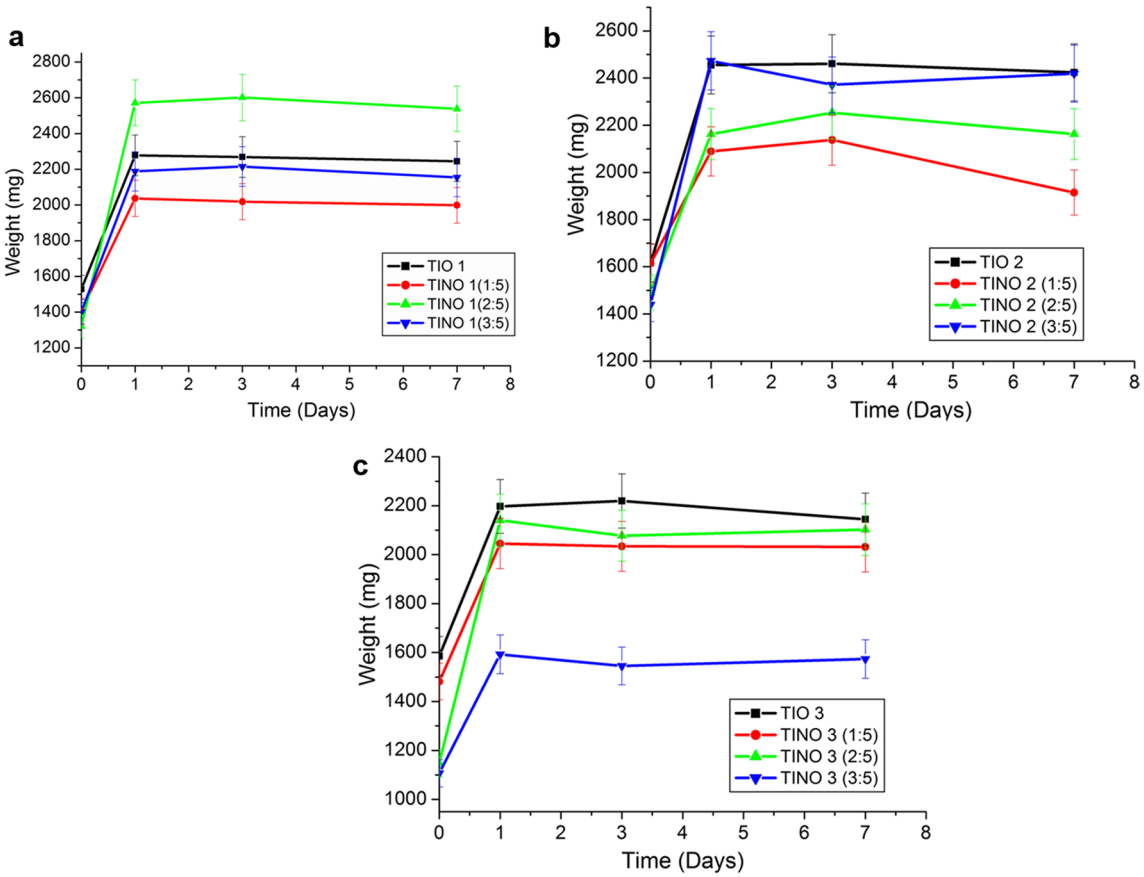

Fig. 7 Degradation and swelling profile for **a** TIO 1, SLN: TINO 1 (1:5), (2:5) and (3:5). Standard deviation <131 in all cases (N=3) **b** TIO 2, SLN: TINO 2 (1:5), (2:5) and (3:5). Standard deviation <124 in all cases (N=3) **c** TIO 3, SLN: TINO 3 (1:5), (2:5) and (3:5). Standard deviation <111 in all cases (N=3)

with a higher concentration of SLNs loaded into the TNO, gelation (swelling) increased as a result of altering the pore patterns and diffusivity of the SLNs within the TO network structure [42].

SLNs loaded into variant TNO 2 revealed dissimilar biodegradation patterns over TNO 1. Figure 7b shows that with an increase of SLN:TO ratio, a significant weight increase of TNO 2 samples occurred after day 1. Furthermore, the rate of swelling (gelation) of the TO and TNO variants on day 1 also had an increased weight proportional to the SLN:TO ratio. Subsequently, at day 3, a decreased weight of TO 2 and TNO 2 variants was observed with a trend for TNO 2 proposing gradual biodegradation of the samples. TNO 2 (1:5) had the lowest weight recorded (1918.02 mg) with TNO 2 (2:5) and TNO (3:5) having final weights of 2159.27 mg and 2417.29 mg, respectively. This suggested once again that the higher SLN:TO ratio produced slower biodegradation and more sustained 5FU release for TNO 2 (1:5, 2:5, and 3:5) at 67.30%, 43.5%, and 41.76% on day 7, respectively.

The biodegradation study of TNO 3 Fig. 7c conformed to a similar pattern as variant TNO 1 with the TNO 3 (2:5) variant having the slowest biodegradation followed by TNO 3 (1:5) and TNO 3 (3:5). It was also observed that there was a substantial increase in the weight (gelation phase) of all TO samples at day 1 followed by a gradual decrease in weight (biodegradation). This is suggestive of an oscillating hydrodynamic pattern for all TNO variants. However, in particular, TO 3 revealed less oscillation with an increase up to day 3 followed by a sharper decrease in weight. The presences of the SLNs also seemed to have prolonged the biodegradation rate [13]. Furthermore, a higher SLN:TO ratio decreased the swelling ability (gelation) particularly of TO 3 due to the SLN's displacing fluid within the gel network.

In Vitro Release Assessment of 5FU from the SLN's and TNO System

Figure 8 represents the release profiles of 5FU from the SLN:TIO variants within the ratios of 1:5 to 3:5. The overall trend in the 5FU release profiles from variants TNO 1-3 showed an initial burst phase of day 1 followed by sustained release over the next 14 days. In the release profiles shown

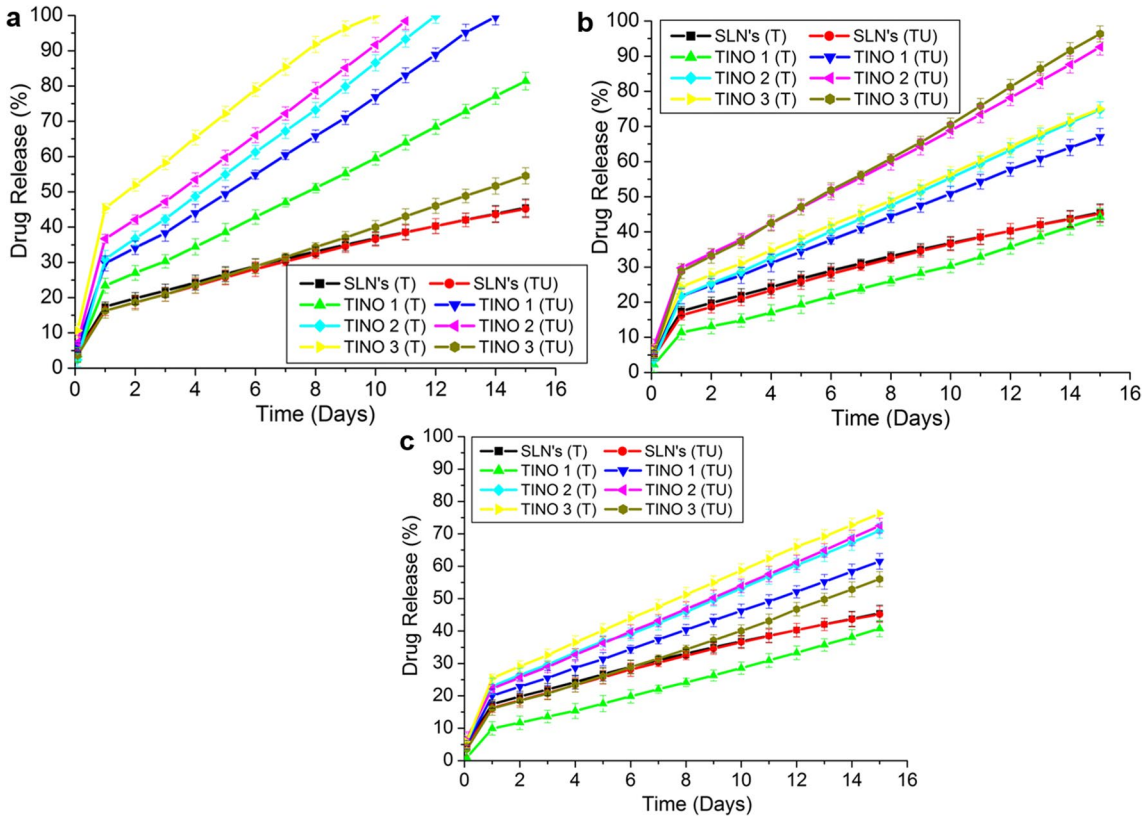

Fig. 8 Drug release profiles for **a** 1:5 SLN: TIO ratio for TINO 1, TINO 2, and TINO 3 (T, thermal; TU, thermal + ultrasound). Standard deviation < 2.5 in all cases (N=3) **b** 2:5 SLN: TIO ratio for TINO 1, TINO 2, and TINO 3. Standard deviation < 2.5 in all cases (N=3) **c** 3:5 SLN: TIO ratio for TINO 1, TINO 2, and TINO 3. Standard deviation < 2.5 in all cases (N=3)

in Fig. 8a, SLNs had the slowest release compared from the TNO variant due to the gelation phenomenon discussed by Yadav and co-workers (2013) [43], i.e., when SLNs are disperse, they undergo rapid crystallization resulting in slower 5FU release [44]. Incorporating the SLNs into the TO increases the release of 5-FU hence overcoming the challenge of gelation [45]. In Fig. 8a, variants TNO 1 and 2 responded to single (thermal (T)) and combined (thermal-ultrasound (TU)) stimuli. TNO variants exposed to the combined stimuli (TU) had a higher rate of 5-FU release over the single stimulus (T). However, findings on variant TNO 3 contradicted the patterns observed for variants TNO 1 and 2. TNO 3 when exposed to the combined stimuli (TU) responded significantly less than with the single stimulus (T) and with a higher release of 5-FU. Hence, incorporating the SLNs within the TNO formulation relaxed the organogel network opening diffusivity pathways for higher 5-FU release [45]. Interestingly, the physical/chemical and internal/external interactions within this network provided precise stimulus and control of 5-FU release from within the formulation [45].

In Fig. 8b, it can be noted that the SLNs revealed the same release pattern observed in Fig. 8a with an initial burst effect on day 1 followed by a steady 5-FU release phase up to day 15. When analyzing all TNO variants, 5-FU was released in a similar pattern when exposed to either the single or combined stimuli, i.e., TNO variants exposed to the combined stimuli (TU) released a higher amount of 5-FU than the single stimulus (T). TNO 1 had the lowest release of 5-FU over the 15-day period and provided the most sustained release profile of all three TNO variants with only 44.29% of 5-FU released under a single stimulus (T) and 67.13% released in the presence of the combined stimuli (TU).

TNO 2 released 5-FU at 74.38% and 92.54% for the single stimulus (T) and combined stimuli (TU) at day 15, respectively. In this ratio of SLN:TO, TNO 3 superseded the 5-FU release of variants TNO 1 and 2 by releasing 75.16% with the single stimulus (T) and 96.43% with the combined stimuli (TU) by day 15. When comparing the overall release of 5-FU in Fig. 8a, Fig. 8b shows desirable sustained release as a trend for all variants suggesting that an increase of SLNs loaded within the TO produces a more sustained release effect [45].

Observations of 5-FU release patterns in Fig. 8c (SLN:TIO at ratio 3:5) can be corroborated with the data presented in Fig. 8b (SLN:TIO at ratio 2:5). The SLNs

released 45.32% of 5-FU by day 15 (Fig. 8a and b). Variants TNO 1 and 2 demonstrated the desired release patterns for cervical cancer intervention [45] while TNO 3 demonstrated contrary behavior with single stimulation (T) presenting a 20.38% higher release of 5-FU by day 15 compared with the combined stimuli (TU) (Fig. 8c).

TNO 1 had a significant difference (±20%) in 5-FU release between the single stimulus (T) (40.66%) and the combined stimuli (TU) (61.35%) by day 15 whereas TNO 2 demonstrated only a 2.27% difference between the single (T) (70.67%) and combined (TU) (72.4%) stimuli. It can be noted that the % 5-FU release shown in Fig. 8c decreased significantly in comparison to Fig. 8a and b. Essentially, the 5-FU release patterns from the TNO mirrored the pure SLNs substantiating to increase the SLN:TO ratio to modulate 5-FU release. In addition, the release of 5-FU from the TNO variants progressed to a steady linear release rate as the SLN concentration increased.

Conclusions

SLNs assembled into TNO variants were prepared and characterized for their *in situ* application to the cervix as a potential site-specific treatment for cervical cancer. In keeping with the objective of achieving stimuli-responsive site-specific and sustained release of 5-FU from the TNO variants, the formulations were augmented by introducing thermal (T) and/or ultrasound (U) responsivity to preferentially increased 5-FU release when applied to the site. Stable 5-FU-loaded SLNs were successfully produced with desirable micromeritic and morphological stability before incorporation into three TNO variants to assess 5-FU release in the presence of single (T)/combined (TU) stimuli. Results revealed that 5-FU was released from the TNO in a sustained release manner over 15 days in simulated cervical fluid. The release rate was primarily influenced by the SLN:TO ratio to produce controlled drug release in tandem with system biodegradation and hydrodynamic influx. Variants TNO 1 and 2 presented the most desired results in terms of controlled 5-FU release under combined thermo-sonic (TU) stimuli and are most promising for superior site-specific delivery of 5-FU to cancerous cervical tissue.

Acknowledgements The authors would like to acknowledge Professor Viness Pillay who sadly passed away (1970–2020) for his contributions to this project.

Author Contribution YEC conceived and designed the work. AZ and SAA acquired, analyzed, interpreted data, and drafted the work, while YEC revised and critically reviewed the work for important intellectual content and gave final approval of the version for publication.

Funding Open access funding provided by University of the Witwatersrand. The authors are grateful for the funding received from the National Research Foundation (NRF) of South Africa.

Declarations

Conflict of Interest The authors declare no competing interests.

References

1. Jin C, Wang K, Oppong-Gyebi A, Hu J. Application of nanotechnology in cancer diagnosis and therapy - a mini-review. Int J Med Sci. 2020;17:2964–73. https://doi.org/10.7150/ijms.49801.
2. Coccia M, Wang L. Path-breaking directions of nanotechnology-based chemotherapy and molecular cancer therapy. Technol Forecast Soc Change. 2015;94:155–69. https://doi.org/10.1016/j.techfore.2014.09.007.
3. Patra JK, Das G, Fraceto LF, Campos EVR, Rodriguez-Torres MDP, Acosta-Torres LS, Diaz-Torres LA, Grillo R, Swamy MK, Sharma S, Habtemariam S, Shin H-S. Nano based drug delivery systems: recent developments and future prospects. J Nanobiotechnology. 2018;16:71. https://doi.org/10.1186/s12951-018-0392-8.
4. Su S, Kang PM. Recent advances in nanocarrier-assisted therapeutics delivery systems. Pharmaceutics. 2020;12:837. https://doi.org/10.3390/pharmaceutics12090837.
5. Yuan Q, Han J, Cong W, Ge Y, Ma D, Dai Z, Li Y, Bi X. Docetaxel-loaded solid lipid nanoparticles suppress breast cancer cells growth with reduced myelosuppression toxicity [Erratum]</p>. Int J Nanomedicine. 2020;14:9877–8. https://doi.org/10.2147/IJN.S242262.
6. Safari J, Zarnegar Z. Advanced drug delivery systems: nanotechnology of health design A review. J Saudi Chem Soc. 2014;18:85–99. https://doi.org/10.1016/j.jscs.2012.12.009.
7. Mountzios G, Soultati A, Pectasides D, Dimopoulos MA, Papadimitriou CA. Novel approaches for concurrent irradiation in locally advanced cervical cancer: platinum combinations, non-platinum-containing regimens, and molecular targeted agents. Obstet Gynecol Int. 2013;2013:536765. https://doi.org/10.1155/2013/536765.
8. Rahangdale L, Lippmann QK, Garcia K, Budwit D, Smith JS, van Le L. Topical 5-fluorouracil for treatment of cervical intraepithelial neoplasia 2: a randomized controlled trial. Am J Obstet Gynecol. 2014;210(314):e1–314.e8. https://doi.org/10.1016/j.ajog.2013.12.042.
9. Kakadia PG, Conway BR. Solid lipid nanoparticles: a potential approach for dermal drug delivery. Am J Pharmacol Sci. 2015;2:1–7. https://doi.org/10.12691/ajps-2-5A-1.
10. Dolatabadi JEN, Valizadeh H, Hamishehkar H. Solid lipid nanoparticles as efficient drug and gene delivery systems: recent

breakthroughs. Adv Pharm Bull. 2015;5:151–9. https://doi.org/10.15171/apb.2015.022.
11. Thakor AS, Gambhir SS. Nanooncology: the future of cancer diagnosis and therapy, CA. Cancer J Clin. 2013;63:395–418. https://doi.org/10.3322/caac.21199.
12. Kumar A, Sawant KK. Solid lipid nanoparticle-incorporated gel: the future treatment for skin infections? Nanomed. 2013;8:1901–3. https://doi.org/10.2217/nnm.13.171.
13. Dorraj G, Moghimi HR. Preparation of SLN-containing thermoresponsive in-situ forming gel as a controlled nanoparticle delivery system and investigating its rheological, thermal and erosion behavior. Iran J Pharm Res IJPR. 2015;14:347–58.
14. Bhaskar K, Anbu J, Ravichandiran V, Venkateswarlu V, Rao YM. Lipid nanoparticles for transdermal delivery of flurbiprofen: formulation, in vitro, ex vivo and in vivo studies. Lipids Health Dis. 2009;8:6. https://doi.org/10.1186/1476-511X-8-6.
15. Nishiyama K. Organogels and hydrogels: functions and structure governed by interactions between gelators and solvents. In: Nishiyama K, Yamaguchi T, Takamuku T, Yoshida N, editors. Mol. Basics Liq. Singapore: Liq.-Based Mater., Springer Nature; 2021. p. 419–37. https://doi.org/10.1007/978-981-16-5395-7_15.
16. Bai B, Li Z, Wang H, Li M, Ozaki Y, Wei J. Exploring the difference in xerogels and organogels through in situ observation. R. Soc. Open Sci. 2018;5:170492. https://doi.org/10.1098/rsos.170492.
17. Patel MN, Lakkadwala S, Majrad MS, Injeti ER, Gollmer SM, Shah ZA, Boddu SHS, Nesamony J. Characterization and evaluation of 5-fluorouracil-loaded solid lipid nanoparticles prepared via a temperature-modulated solidification technique. AAPS PharmSciTech. 2014;15:1498–508. https://doi.org/10.1208/s12249-014-0168-x.
18. Miller D, Smith N, Bailey M, Czarnota G, Hynynen K, Makin I. Overview of therapeutic ultrasound applications and safety considerations. J Ultrasound Med Off J Am Inst Ultrasound Med. 2012;31:623–34.
19. Rapoport N, Payne A, Dillon C, Shea J, Scaife C, Gupta R. Focused ultrasound-mediated drug delivery to pancreatic cancer in a mouse model. J Ther Ultrasound. 2013;1:11. https://doi.org/10.1186/2050-5736-1-11.
20. Couture O, Foley J, Kassell NF, Larrat B, Aubry J-F. Review of ultrasound mediated drug delivery for cancer treatment: updates from pre-clinical studies. Transl Cancer Res. 2014;3:10.21037/3354.
21. Burmeister CA, Khan SF, Schäfer G, Mbatani N, Adams T, Moodley J, Prince S. Cervical cancer therapies: current challenges and future perspectives. Tumour Virus Res. 2022;13:200238. https://doi.org/10.1016/j.tvr.2022.200238.
22. Mishra V, Bansal KK, Verma A, Yadav N, Thakur S, Sudhakar K, Rosenholm JM. Solid lipid nanoparticles: emerging colloidal nano drug delivery systems. Pharmaceutics. 2018;10:191. https://doi.org/10.3390/pharmaceutics10040191.
23. Maji R, Dey NS, Satapathy BS, Mukherjee B, Mondal S. Preparation and characterization of Tamoxifen citrate loaded nanoparticles for breast cancer therapy. Int J Nanomedicine. 2014;9:3107–18. https://doi.org/10.2147/IJN.S63535.
24. Awotwe-Otoo D, Zidan AS, Rahman Z, Habib MJ. Evaluation of anticancer drug-loaded nanoparticle characteristics by nondestructive methodologies. AAPS PharmSciTech. 2012;13:611–22. https://doi.org/10.1208/s12249-012-9782-7.
25. Alphandéry E. Ultrasound and nanomaterial: an efficient pair to fight cancer. J Nanobiotechnol. 2022;20:139. https://doi.org/10.1186/s12951-022-01243-w.
26. Martin DK. Low-frequency ultrasound can drive the transport of nanoparticles and molecules in polymer gels for biotechnology applications. EuroBiotech J. 2019;3:1–9. https://doi.org/10.2478/ebtj-2019-0001.
27. Shi L, Li Z, Yu L, Jia H, Zheng L. Effects of surfactants and lipids on the preparation of solid lipid nanoparticles using double emulsion method. J Dispers Sci Technol. 2011;32:254–9. https://doi.org/10.1080/01932691003659130.
28. Abbaspour M, Makhmalzadeh BS, Arastoo Z, Jahangiri A, Shiralipour R. Effect of anionic polymers on drug loading and release from clindamycin phosphate solid lipid nanoparticles. Trop J Pharm Res. 2013;12:477–82. https://doi.org/10.4314/tjpr.v12i4.5.
29. Sharma D, Maheshwari D, Philip G, Rana R, Bhatia S, Singh M, Gabrani R, Sharma SK, Ali J, Sharma RK, Dang S. Formulation and optimization of polymeric nanoparticles for intranasal delivery of lorazepam using Box-Behnken design: in vitro and in vivo evaluation. BioMed Res Int. 2014;2014:156010. https://doi.org/10.1155/2014/156010.
30. Abdellatif AAH, Tawfeek HM. Transfersomal nanoparticles for enhanced transdermal delivery of clindamycin. AAPS PharmSciTech. 2016;17:1067–74. https://doi.org/10.1208/s12249-015-0441-7.
31. Honary S, Zahir F. Effect of zeta potential on the properties of nano-drug delivery systems - a review (Part 1). Trop J Pharm Res. 2013;12:255–64. https://doi.org/10.4314/tjpr.v12i2.19.
32. Grainger SJ, Serna JV, Sunny S, Zhou Y, Deng CX, El-Sayed MEH. Pulsed ultrasound enhances nanoparticle penetration into breast cancer spheroids. Mol Pharm. 2010;7:2006–19. https://doi.org/10.1021/mp100280b.
33. López-García R, Ganem-Rondero A. Solid lipid nanoparticles (SLN) and nanostructured lipid carriers (NLC): occlusive effect and penetration enhancement ability. J Cosmet Dermatol Sci Appl. 2015;5:62–72. https://doi.org/10.4236/jcdsa.2015.52008.
34. Khadka P, Ro J, Kim H, Kim I, Kim JT, Kim H, Cho JM, Yun G, Lee J. Pharmaceutical particle technologies: an approach to improve drug solubility, dissolution and bioavailability, Asian. J Pharm Sci. 2014;9:304–16. https://doi.org/10.1016/j.ajps.2014.05.005.
35. Narala A, Veerabrahma K. Preparation, characterization and evaluation of quetiapine fumarate solid lipid nanoparticles to improve the oral bioavailability. J Pharm. 2013;2013:e265741. https://doi.org/10.1155/2013/265741.
36. Ahad N, Saion E, Gharibshahi E. Structural, thermal, and electrical properties of PVA-sodium salicylate solid composite polymer electrolyte. J Nanomater. 2012;2012:e857569. https://doi.org/10.1155/2012/857569.
37. Olukman M, Şanlı O, Solak EK. Release of anticancer drug 5-fluorouracil from different ionically crosslinked alginate beads. J Biomater Nanobiotechnol. 2012;3:469–79. https://doi.org/10.4236/jbnb.2012.34048.
38. Tahan Latibari S, Mehrali M, Mehrali M, Mahlia TMI, Metselaar HSC. Facile preparation of carbon microcapsules containing phase-change material with enhanced thermal properties. Scientific World J. 2014;2014:379582. https://doi.org/10.1155/2014/379582.
39. Manjunath A, Deepa T, Supreetha NK, Irfan M. Studies on AC Electrical conductivity and dielectric properties of PVA/NH4NO3 solid polymer electrolyte films. Adv Mater Phys Chem. 2015;5:295–301. https://doi.org/10.4236/ampc.2015.58029.
40. Nair LK, Jagadeeshan S, Nair SA, Kumar GV. Biological evaluation of 5-fluorouracil nanoparticles for cancer chemotherapy and its dependence on the carrier, PLGA. Int J Nanomed. 2011;6:1685–97. https://doi.org/10.2147/IJN.S20165.
41. Horvat G, Pantić M, Knez Ž, Novak Z. A brief evaluation of pore structure determination for bioaerogels. Gels. 2022;8:438. https://doi.org/10.3390/gels8070438.
42. Zhang D, Wei J, Fang X. Study on the variation of rock pore structure after polymer gel flooding. E-Polym. 2020;20:32–8. https://doi.org/10.1515/epoly-2020-0004.
43. Yadav YJ, Heinrich B, De Luca G, Talarico AM, Mastropietro TF, Ghedini M, Donnio B, Szerb EI. Chromonic-like physical luminescent gels formed by ionic octahedral iridium(III) complexes in

diluted water solutions. Adv Opt Mater. 2013;1:844–54. https://doi.org/10.1002/adom.201300236.
44. Lingayat VJ, Zarekar NS, Shendge RS. Solid lipid nanoparticles: a review. Nanosci Nanotechnol Res. 2017;4:67–72. https://doi.org/10.12691/nnr-4-2-5.
45. Entezar-Almahdi E, Mohammadi-Samani S, Tayebi L, Farjadian F. Recent advances in designing 5-fluorouracil delivery systems: a stepping stone in the safe treatment of colorectal cancer. Int J Nanomed. 2020;15:5445–58. https://doi.org/10.2147/IJN.S257700.